# Design of an LED driver based on hysteretic-current-control mode in a 0.6 $\mu$m BCD process*

Liu Lianxi(刘帘曦)†, Zhu Zhangming(朱樟明), and Yang Yintang(杨银堂)

Institute of Microelectronics, Xidian University, Xi'an 710071, China

**Abstract:** Based on the 0.6 $\mu$m BCDMOS process a hysteretic-current-control mode white light LED driver with high accuracy and efficiency is presented. The driver can work with a 6–40 V power supply, the maximum output current is up to 1.0 A, the maximum switching frequency is up to 1 MHz, the output current error is less than $\pm$5%, and the efficiency is greater than 80%. The circuit details of the high-side-current sensor and high-speed comparator, which greatly affect the accuracy of the whole driver, are emphasized. Then, the simulation and test results of this work are presented.

**Key words:** hysteretic-current-control; output-current error; high-side-current sensing; high-speed comparator
**DOI:** 10.1088/1674-4926/33/4/045005 **EEACC:** 2520

## 1. Introduction

As a fourth-generation lighting device, the LED (light emitting diode) is considered as a historical leap in lighting history[1, 2]. Its characteristics are high luminance, energy-saving effect, long life service, nice light color and high stability. As a result, the popularity of the LED will create an extensive market space for LED drivers[2, 3]. In the field of LED lighting, it is important to choose a good driver IC for the characteristics of energy-saving and long life of the LED. Some essential issues should be resolved for high-power LED driver ICs, such as voltage step-down, constant current, response time, output current accuracy and high conversion efficiency[4]. The traditional voltage mode PWM modulation solution has the characteristics of slow response and poor consistency of the output current. Therefore, the solution of high-precision current-mode drive is becoming the hot issue for LED lighting[5]. Studies have shown that the hysteretic-current-control model is suitable for a high-accuracy driver system with a wide voltage supply range[6]. In this work, the main BUCK topology based on current continuous-conduction mode (CCM) is proposed, of which the feedback control mode is the hysteretic current control.

## 2. The overall circuit structure and working principle

The system block diagram of the proposed hysteretic-current-control mode LED driver is shown in Fig. 1, and the whole system is a single-loop current control system. The control signal is input from the ADJ pin. According to the application, this pin can be left floating, or DC voltage or PWM signal. The error amplifier (Err AMP) and the sampling resistor ($R_s$) detect the current change in LED, and amplify it. Amplified current change is compared with the control signal form ADJ pin by a comparator (PWM Comp) to generate the PWM signal to drive NDMOSFET (MN). To improve device reliability, a band gap voltage source (Band gap), an over temperature protection module (Over Temp) and a low pass filter (LPF) are integrated internally.

To facilitate understanding, assume that the ADJ pin is floating, and ADJ voltage $V_{\rm ADJ}$ is directly added to the PWM comparator's non-inverting input. When the input voltage $V_{\rm IN}$ is applied to the circuit, the initial current flowing through inductor $L_1$ and resistor $R_{\rm S}$ is 0, at this point, the current sensor circuit does not work. The PWM comparator inverting input is equivalent to short to ground, so the output is high. This output signal will go through the buffer to turn on the power switch MN, and pull the LX pin down. Then, the current from $V_{\rm IN}$ pin flows through $R_{\rm S}$, $L_1$ and LED to ground, and the inductor current will gradually increase. The increase slope of the current is decided by the value of $L_1$ and $V_{\rm IN}$. At the same time, the ramp current will accordingly generate a ramp voltage ($V_{\rm SENCE}$) across the resistor $R_{\rm S}$. The voltage ($V_{\rm SENCE}$), which is related to the supply voltage $V_{\rm IN}$, is converted into a current flowing through the resistor $R_1$, while flowing through the resistors $R_2$ and $R_3$. Since $R_2$ and $R_3$ are in series between the PWM comparator inverting terminal and ground, the current $V_{\rm SENCE}/R_1$ will cause the PWM comparator inverting voltage to begin to increase from 0. When the voltage of the PWM comparator inverting input rises to the threshold voltage ($V_{\rm ADJ}$), the output voltage of the comparator will change from high to low, which makes the power switch MN turn off.

The PWM comparator output also controls the other NMOS switch M3, which can be shorted or connected to the resistor $R_3$ to generate the hysteresis in the comparator. The hysteretic value, which can be set by the resistance of $R_3$, is about 15% of $V_{\rm ADJ}$. When the power switch is turned on, $R_3$ is shorted, and when off, $R_3$ is in series with $R_2$. Therefore, current-sense signal $V_{\rm SENCE}$ and $R_2$, $R_3$ can be expressed as:

* Project supported by the National Natural Science Foundation of China (No. 61006028), the Xi'an Applied Materials Innovation Fund, China (No. XA-AM-201010), and the National Science Fund for Distinguished Young Scholars, China (No. 60725415).
† Corresponding author. Email: lxliu@mail.xidian.edu.cn
Received 27 August 2011, revised manuscript received 22 October 2011 

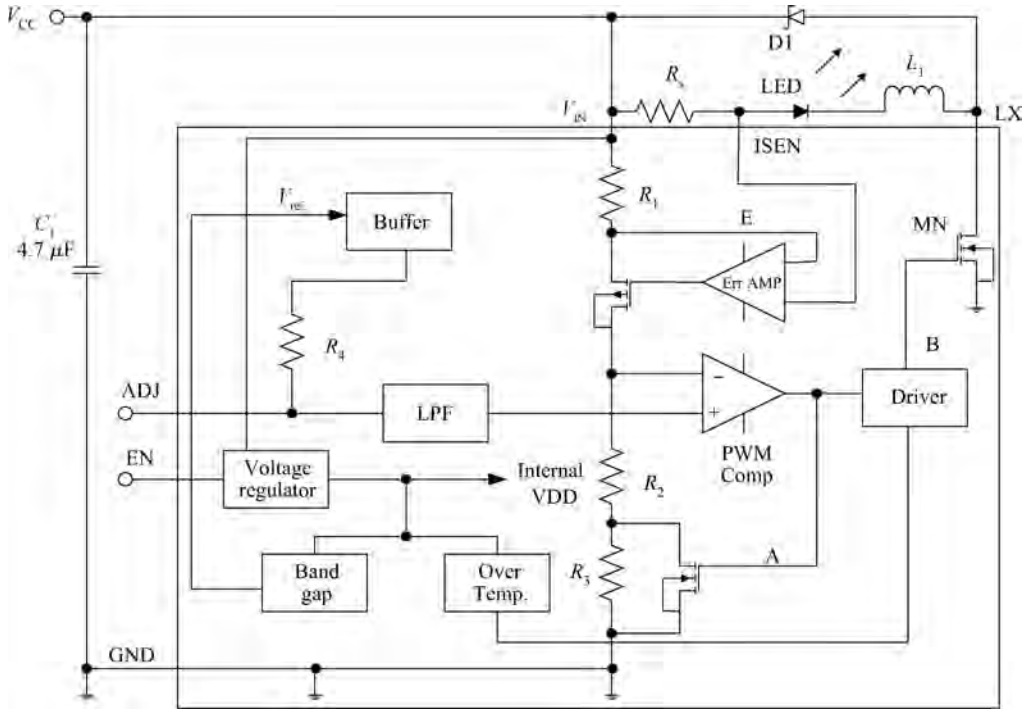


Fig. 1. Block diagram of the proposed LED driver system.

$$V_{\text{sense}} = \frac{R_2 + R_3}{R_1}(V_{\text{IN1}} - V_{\text{IN2}}). \tag{1}$$

That is to say:

$$\begin{cases} V_{\text{sense}} = \dfrac{R_2}{R_1}(V_{\text{IN1}} - V_{\text{IN2}}), & \text{power switch is on,} \\ V_{\text{sense}} = \dfrac{R_2 + R_3}{R_1}(V_{\text{IN1}} - V_{\text{IN2}}), & \text{power switch is off.} \end{cases} \tag{2}$$

When MN is turned off, the inductor current flows through the LED and freewheeling diode D1 back into the $V_{\text{IN}}$. In this case, the inductor current will gradually decrease, of which the decline slope is determined by the LED and the diode forward voltage, and the ramp current flowing through $R_1$ will make the voltage of the PWM comparator inverting drop. When the voltage on comparator inverting terminal drops to the threshold ($V_{\text{ADJ}}$), the output will change again, from low to high, and so the new cycle begins again. PWM comparator input will change in the $\pm 15\%$ of $V_{\text{ADJ}}$. Thus, the LED-driver-current accuracy in the hysteretic-current-control mode is mainly decided by the accuracy of the high-side current sensing circuit and the delay of hysteretic comparator[7, 8].

## 3. High-side-current sensing circuit

For an LED driver system, especially a very wide voltage input range, hysteretic-control mode has a comparative advantage on the current accuracy[9]. The current accuracy of the whole system depends mainly on the current sensing accuracy and the delay within the system. Thus, a high accuracy load current sensing circuit is required for the driver based on hysteretic-current-control mode.

The proposed high-side current sensing circuit in this driver is shown in Fig. 2, M14–M18 constitute a current bias circuit to provide the PTAT current for the other circuit, M5–M8 constitute a cascode-current-source, where the two branch currents are kept the same ($I_1 = I_2$). In this case, since the bias current in the two branches are the same, the cascade-current-mirror consisted of M1–M4 shows the effect of "voltage mirror[10]". This will make the point A and point B in the same potential, when the resistance value of $R_1$ is equal to that of $R_2$. According to the current relationship, Equation (3) can be deduced as:

$$V_{\text{out}} = \frac{R_3}{R_1}(V_{R_s} - V_{\text{A}} + V_{\text{B}}) = \frac{R_3}{R_1}V_{R_s}. \tag{3}$$

Equation (3) shows that the voltage across the sensing resistor $R_s$ is magnified by $R_3/R_1$ times before being outputted. Therefore, the current accuracy is significantly affected by the mismatch between points A and B. According to Eq. (3), the accuracy can be expressed as:

$$\eta = \frac{V_{\text{A}} - V_{\text{B}}}{|V_{R_s}|} \times 100\%. \tag{4}$$

In Fig. 2, $V_{\text{in1}}$ is directly connected to the power supply. The charge and discharge of the inductive make the $V_{\text{in2}}$ voltage constantly change. The amplitude of this change is very small, but the frequency is very high. At the same time, the voltage variation at $V_{\text{in2}}$ will result the voltage change at point B. So, the voltage at point A needs to be adjusted quickly to ensure that the voltages of points A and B are always equal, that is to say, $V_{\text{in1}}$ should change quickly following the change of $V_{\text{in2}}$. This feature can be achieved to use a negative feedback structure, as shown in Fig. 2. When there is a small fluctuation in voltage of $V_{\text{in2}}$, a change will occur at the voltage of point B, which is magnified by the two stage common-gate amplifier

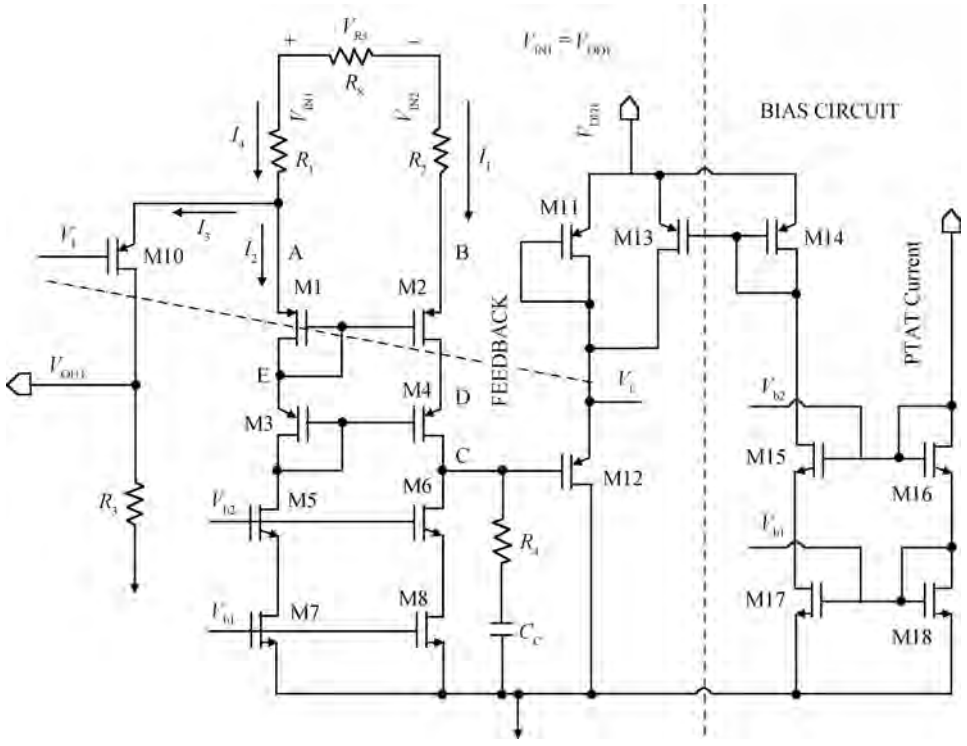


Fig. 2. Schematic of the high-side current sensor with high-accuracy.

consisted of M2 and M4, and then makes the voltage at point C change too. M10–M13 constitute a source follower to detect the voltage change at point C, and then adjust the voltage at point A to keep the balance of the two branches. The gain and bandwidth of the loop directly affect the accuracy and sensitivity of the whole current sensor. As zero-pole compensation devices, a zero-regulator resistor $R_4$ and a compensation capacitor $C_C$ are introduced in the loop to ensure high unit-gain bandwidth and better stability. Therefore, there are two pole points and a zero point at point C, and then, the pole and zero point expression as:

$$\begin{cases} \omega_{p1} \approx -1/R_O C_C, \\ \omega'_{p2} \approx -1/R_4 C_O, \\ \omega_z = -/R_4 C_C. \end{cases} \tag{5}$$

In Eq. (5), $R_O$ and $C_O$ are respectively the output resistance and parasitic capacitance at point C without compensation. Because the second pole $\omega'_{p2}$ is very far away from the origin, it can be ignored.

As shown in Fig. 2, in the loop, the small signal transmits from $V_{in1}$ to point C, respectively through a two-stage common-gate amplifier which is consisted of M2 and M4, and a two-stage source follower consisted of M10–M13, then to point A. So the gain of open-loop is:

$$A_V \approx \frac{g_{m2} g_{m4} r_{o2} r_{o4}}{1 + g_{m2} R_{1,2}} \frac{g_{m12}}{g_{m11} + g_{m12}} \frac{g_{m9} R_{1,2} r_{o10}}{g_{m9} R_{1,2} r_{o10} + r_{o9}}. \tag{6}$$

And the main pole and zero points are:

$$\begin{cases} \omega_{p1} \approx -1/R_O C_C \\ \omega_{p2} = -g_{m4}/C_2 \\ \omega_z = -1/R_4 C_C. \end{cases} \tag{7}$$

It can be seen from Eqs. (6) and (7) that the value of resistors $R_1$ and $R_2$ will greatly affect the loop gain, which should be selected carefully. Additionally, the gate and drain of M11 are shorted in Fig. 2, which make the output impedance at point C reduce. That is to say, the pole at point $V_1$ will be pushed far away from the origin, which could ensure better stability of the whole loop.

## 4. High-speed comparator

A high-speed comparator generally uses a pre-amplifier to magnify the differential input signal, and then a judgment-stage circuit to compare the amplified signal with a reference, finally an output-stage to output a high or low signal. To reduce the total delay of a comparator, the characters of low-gain and wide bandwidth are required by the pre-amplifier. Figure 3 shows the proposed high-speed comparator. M20–M24 constitute a fully differential structure as the pre-amplifier, M25–M31 as the judgment-stage, the gate and drain of M29 and M30 are coupled which forms a positive feedback, and M32–M39 constitute a self-bias amplifier as the output stage of the comparator.

Figure 4 shows the small-signal model of the side-equivalent-circuit of the judgment stage. In Fig. 3, the gate of M10 is connected to $V_{out2}$, and the phase of $V_{out2}$ voltage is opposite to that of $V_{out1}$ voltage. Therefore, the admittance of M10 is negative, which improves the output impedance, and then increases the gain of judgment stage. The output impedance is:

$$\begin{aligned} R_{OUT} &= \frac{1}{g_{ds26} + g_{ds28} + g_{ds30} + g_{m28} - g_{m30}} \\ &\approx \frac{1}{g_{m28} - g_{m30}}. \end{aligned} \tag{8}$$

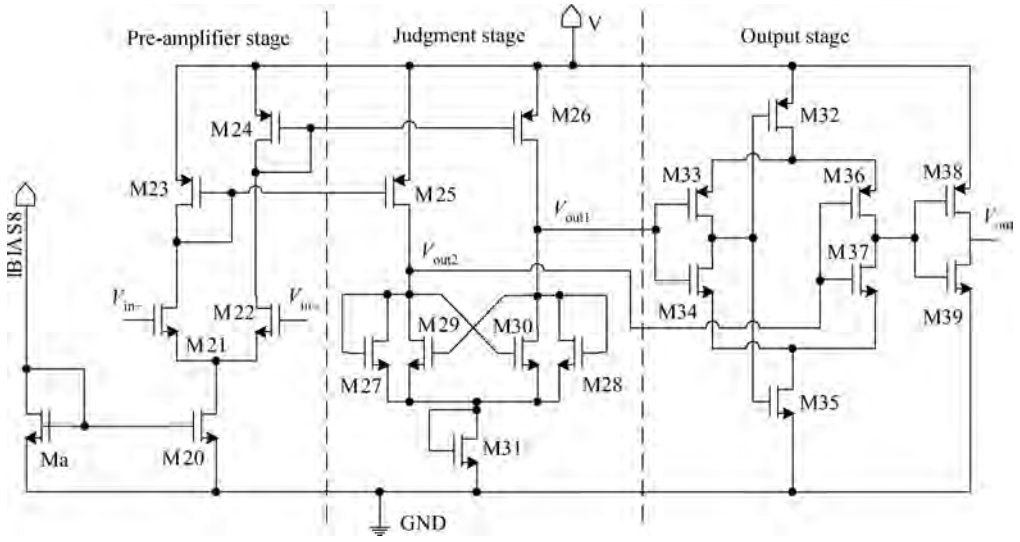


Fig. 3. Schematic of the high-speed comparator.

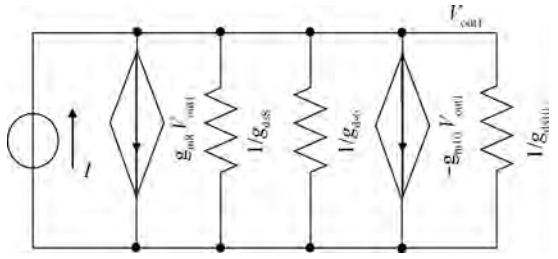

Fig. 4. Small-signal model of side-circuit in judgment stage.

So, the gain of pre-amplifier and judgment-stage is:

$$A_{\mathrm{V}} \approx \frac{g_{\mathrm{m21}}}{g_{\mathrm{m28}} - g_{\mathrm{m30}}}. \tag{9}$$

And the transmission delay of the comparator can be expressed as:

$$t = \frac{t_{\mathrm{p}}}{|p_1|} = \frac{1}{|p_1|\sqrt{mk}} = \frac{\sqrt{V_{\mathrm{OH}} - V_{\mathrm{OL}}}}{\sqrt{A_{\mathrm{V0}}}\sqrt{p_1 p_2}\sqrt{V_{\mathrm{in}}}}. \tag{10}$$

In Eq. (10), $t_{\mathrm{p}}$ is the normalized transmission delay, $m = p_2/p_1$, $k = V_{\mathrm{in}}/V_{\mathrm{in(min)}}$, and $V_{\mathrm{in(min)}} = (V_{\mathrm{OH}} - V_{\mathrm{OL}})/A_{\mathrm{V0}}$, is the accuracy of the comparator. $V_{\mathrm{OH}} - V_{\mathrm{OL}}$ is the swing range of the output voltage, and $A_{\mathrm{V0}}$ is the small-signal DC gain of the comparator. With the input voltage $V_{\mathrm{in}}$ (the differential voltage between comparator inputs) increasing, the transmission delay in the comparator will decrease, and the circuit is linear in this condition. But when $V_{\mathrm{in}}$ reaches a certain value, the transmission delay is no longer significantly reduced with $V_{\mathrm{in}}$, and the comparator shows a slew-rate-limited feature. The transmission delay of the proposed comparator is mainly affected by the linear response characteristic, but the slew rate is limited.

## 5. Experimental results

The proposed LED driver circuit has been verified in a 0.6 $\mu$m BCD process. Due to the high output power, the power switch in chip is constituted by 2400 NLDMOS in parallel, and

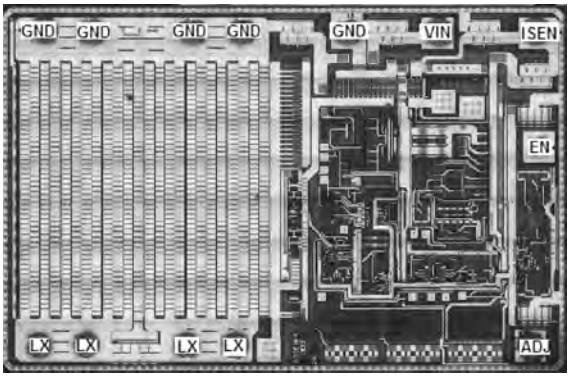


Fig. 5. Photo of the whole die.

the ratio of width to length of each NLDMOS is 50 $\mu$m/1 $\mu$m. The power transistor layout area is so large that it accounts for almost half of entire chip area. The photo of the whole is shown in Fig. 5. The die size is about 1.2 × 1.5 mm$^2$, and the chip package is SOT23-6.

As is shown in Fig. 6, the green module is used to drive a 1-W LED, whose supply voltage range of 6–40 V, constant current value of about 360 mA; the blue module is used to drive three 1-W LEDs in series, supply voltage range of 6–40 V, constant current value of about 360 mA; and the red module is used to drive a 3-W LED, supply voltage range of 6–40 V, constant current value of about 1000 mA.

When the sense resistor $R_{\mathrm{S}}$ is 0.13 Ω and the inductor $L_1$ is 47 $\mu$H (Fig. 1), the waves of the output current varying with the supply voltage at different loads are shown in Fig. 7. It can be seen from this figure that the proposed circuit could drive, at most, 11 1-W LEDs in series. The output current changes almost linearly with supply voltage, and the wider the supply voltage range is, the greater the output current range is. Therefore, the power supply voltage range should be properly controlled according to the output current range, especially in the condition that the current accuracy is strictly required.

When the power supply is 40 V, sense resistance is 0.33 Ω, inductance is 47 $\mu$H and load is a 1-W LED, the waveform of

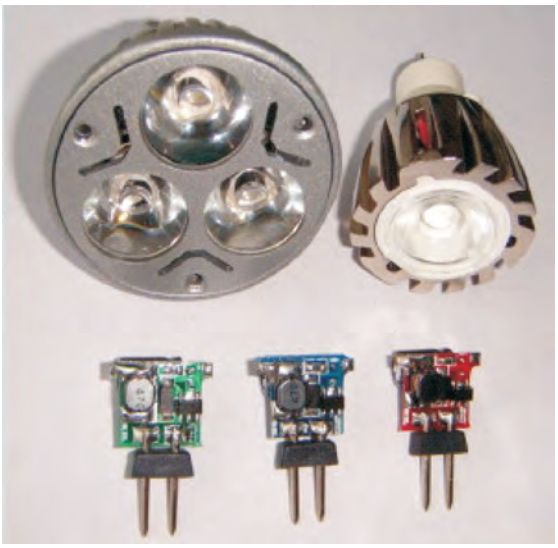

Fig. 6. Photo of MR16 and application modules.

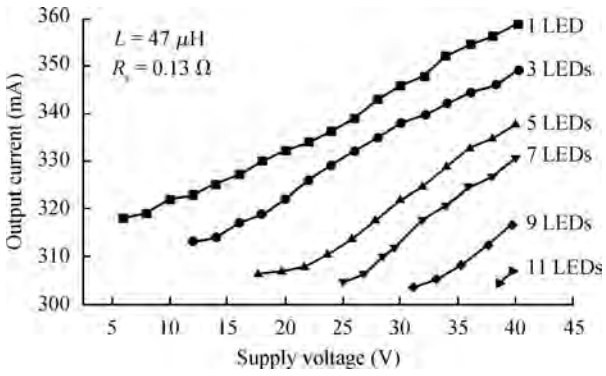


Fig. 7. Output current versus supply voltage at different loads.

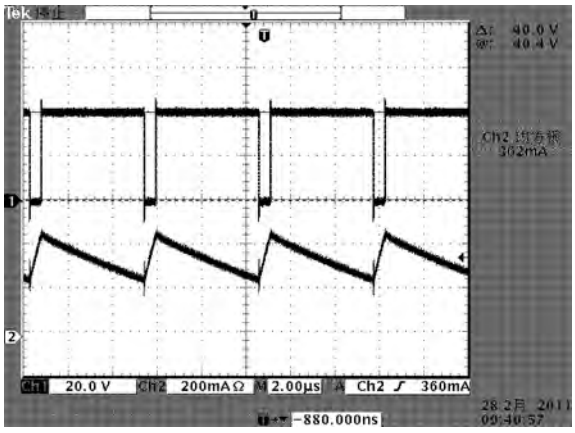


Fig. 8. Waves of MN drain voltage and current in $L$ at $V_{in} = 40$ V.

the power transistor drain voltage and the waveform of the inductor current are shown in Fig. 8. The output current flowing through the LED is about 360 mA, in this condition.

When the sense resistor $R_S$ is 0.13 Ω and the inductor $L_1$ is 47 $\mu$H (Fig. 1), the waveforms of the convention efficiency varying with the supply voltage are shown in Fig. 9. When the load is a 3-W LED, and the supply voltage changes from 18 to 30 V, the efficiency of the system can be up to 80%. When the load is three 3-W LEDs in series, and the supply voltage changes from 22 to 36 V, the efficiency of the system could be up to 90%. Therefore, based on the load, a reasonable choice of the range of the supply voltage can improve the drive efficiency.

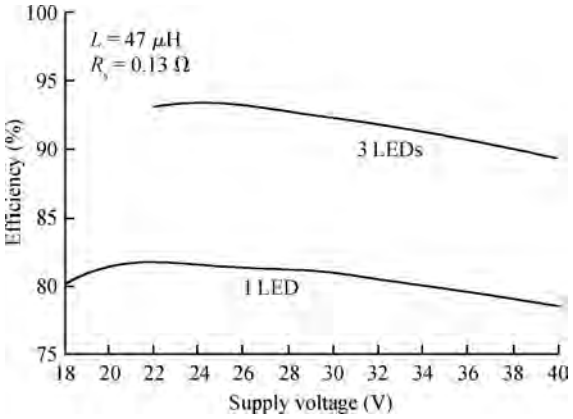


Fig. 9. Measured result of efficiency versus supply voltage at different loads.

Table 1. Some measure results of this chip.

| Parameter | Min | Typ | Max |
|---|---|---|---|
| Output current, $I_{out}$ (mA) | 325 | 330 | 336 |
| Efficiency, Eff (%) | 81 | 85 | 88 |
| Standby current, $I_{DDQ}$ ($\mu$A) | 90 | 100 | 110 |
| Switch resistance, $R_{SW}$ (Ω) | 0.22 | 0.25 | 0.28 |
| Switching frequency, $F_{SW}$ (kHz) | 690 | 800 | 1020 |
| Sensing voltage, $V_{IN} - V_{ISEN}$ (mV) | 87 | 90 | 95 |
| Over temp protection, $T_{SD}$ (℃) | 129 | 140 | 146 |
| Current accuracy, Acc (%) | 3.5 | 4.2 | 5.0 |

Table 1 shows some of the other main measure parameters of the chip in a typical case ($V_{IN}$ is 18 V, room temperature and load is a 1-W LED). Performance comparison with some other references[11−13] is shown in Table 2. The driver in Ref. [11] regulates the current by PFM and PWM dual mode, and has the advantage of conversation efficiency. But due to the voltage control mode and process limitation, the input voltage range is small and the current accuracy is low. Reference [12] shows a low power current sensing circuit for a Buck-Boost LED driver. It is only suitable for low input voltage applications. The circuit proposed in Ref. [13] using pulse current modulator has the characteristics of low static power consumption and small die size. However, also due to process limitations, the input voltage range and output current is relatively small, in addition, the accuracy is not high. Due to the BCD process and the hysteretic-current-control mode, the proposed driver has obvious advantages on input voltage range, output current and output current accuracy.

## 6. Conclusion

The hysteretic-current-control mode has the characteristics of fast transient response and good stability performance, which are the main trending control techniques among LED driver products. This paper presents a hysteretic-current-

Table 2. Comparison with some other references.

| Product name | Control mode | Input range (V) | Current accuracy (%) | Efficiency (%) | Die area (about) ($mm^2$) | Output current (mA) |
|---|---|---|---|---|---|---|
| Ref. [11] | Voltage | 5.0–40 | > 6 | 90 | — | 350 |
| Ref. [12] | Current | < 5 | — | 92 | 2.4 × 2.5 | 350 |
| Ref. [13] | Pulse-current | 4.5–5.5 | — | — | 1.0 × 1.0 | 250 |
| This work | Hysteretic-current | 6.0–40 | 4.2 | 88 | 1.2 × 1.5 | 1000 |

control mode white LED driver based on 0.6 $\mu$m BCD process, and focuses on the high-side current sensor circuit and high-speed comparator. The simulation and test results for the circuit show that the chip can drive 11 1-W LEDs at most by 360 mA current, when the supply voltage is 40 V. When the supply voltage changes from 18 to 40 V, the on-resistance of internal switch NLDMOS is about 0.2 Ω. Typically, the efficiency of the whole system is more than 80%，the output current error is less than ±5%. Therefore, the proposed hysteretic-current-control mode driver can be widely used in white LED lighting because of its high conversion efficiency and high accuracy.

## Acknowledgment

All the writers would like to thank Wang Jianhui of the Chengdu Chip-Rail Tech Co., Ltd, for his great assistance in the application and testing.

## References

[1] Spiazzi G, Buso S, Meneghesso G. Analysis of a high power-factor electronic ballast for high brightness light emitting diodes. 36th IEEE Power Electronics Specialists Conference (PESC) Proc, 2005: 1494

[2] Mineiro Sá E Jr, Agostin E Jr, Bedin J. Design of an electronic driver for LEDs. COBEP 07-9 Brazilian Power Electronics Conference, 2007: 341

[3] Broeck H, Sauerlander G, Vendt M. Power driver topologies and control schemes for LEDs. IEEE Applied Power Electronics Conference (APEC) Proc, 2007: 1319

[4] Li J, Lee F C. New modeling approach and equivalent circuit representation for current-mode control. IEEE Trans Power Electron, 2010, 25(5): 1218

[5] Carraro G. Solving high-voltage off-line HB-LED constant current control-circuit issues. IEEE Applied Power Electronics Conference (APEC) Proc, 2007: 1316

[6] Oh I H. An analysis of current accuracies in peak and hysteretic current controlled power LED drivers. 23rd IEEE Applied Power Electronics Conference and Exposition (APEC), 2008: 572

[7] Trescases O, Prodic'A, Ng W T. Digitally controlled current-mode DC–DC converter IC. IEEE Trans Circuits Syst, 2011, 58(1): 219

[8] Burgyan L, Prinz F. High efficiency LED driver. USA Patent, No. 6690146, Feb 10, 2004

[9] Parayandeh A, Trescases O, Prodic A. 10 MHz peak current mode DC–DC converter IC with calibrated current observer. IEEE Applied Power Electronics Conference and Exposition (APEC), 2011: 897

[10] Chiu H J, Cheng S J. LED backlight driving system for large-scale LCD panels. IEEE Trans Industrial Electron, 2007, 54(5): 2751

[11] Yang Yuan, Song Zhenghua, Gao Yong. A white LED driver based on dual mode switch dimming. Symposium on Photonics and Optoelectronics, 2009: 1

[12] Leung W Y, Man T Y, Chan M. A high-power-LED driver with power-efficient LED-current sensing circuit. 34th European Solid-State Circuits Conference (ESSCIRC), 2008: 354

[13] Lin M S, Chen C L. A LED driver based on pulse current modulator. 26th IEEE Power Electronics Specialists Conference (APEC), 2011: 2054